Resources, Conservation & Recycling 222 (2025) 108466

Contents lists available at ScienceDirect

Resources, Conservation & Recycling

journal homepage: www.sciencedirect.com/journal/resources-conservation-and-recycling

Full length article

Fully upcycling spent ternary cathodes by simultaneously extracting lithium and constructing high performance oxygen evolution catalysts

Chunli Gou [a], Fang Gao [a,b], Mingke Yang [a], Zhihao Zhang [a,*], Chunli Wang [a], Yufang Wang [a], Xinwen Ou [c], Jing Zhang [a,*]

[a] National Engineering Laboratory for VOCs Pollution Control Material & Technology, Research Center for Environmental Material and Pollution Control Technology, University of Chinese Academy of Sciences, Beijing 101408, PR China
[b] Sino-Danish College, University of Chinese Academy of Sciences, Beijing 101408, PR China
[c] School of Physics, Zhejiang University, Hangzhou 310058, PR China

ARTICLE INFO

Keywords:
Spent Ternary Cathodes
Upcycling
Flash Joule Heating
Selective Extraction
Surface Reconstruction
Oxygen Evolution Reaction

ABSTRACT

Recycling spent ternary batteries provides a dual benefit in both addressing environmental concerns and favoring resource utilization. However, conventional recycling strategies suffer from lengthy separation procedures and low recovery efficiency of valuable metals. This work proposed a flash joule heating-based direct conversion strategy to both selectively extract lithium and transform other metals into oxygen evolution reaction (OER) catalyst from the leaching solution of ternary cathodes. In this way, 95.89 % lithium was collected by water-leaching. Meanwhile, a self-supported catalyst was built-up by the remaining solid and covered with multimetallic hydroxide film through surface reconstruction. It exhibited an excellent OER catalytic activity with a low overpotential of 257 mV (vs. reversible hydrogen electrode (RHE)) at 10 mA/cm^2. DFT calculations revealed that Co/Mn in the multimetallic hydroxide enhanced M-O charge transfer. Economic and environmental analysis confirmed its superior sustainability compared with conventional methods. This work established a sustainable and efficient pathway for fully upcycling ternary cathodes.

1. Introduction

The shift of energy structure toward renewable energy has generated a high demand for efficient energy storage materials. Especially with the rapid advancement of electric vehicles, lithium-ion batteries (LIBs) have entered a golden era of development and been wildly adopted (Khan et al., 2023; Li et al., 2022; Yang et al., 2023a). Due to the limited lifespan of only eight to ten years, nearly 11 million tons of LIBs will reach the end-of-life stage by 2030 and turn into potential waste (Chen et al., 2019). The spent LIBs normally contain substantial amounts of lithium and transition metals such as nickel, cobalt, and manganese in the $LiNi_{1-x-y}Co_xMn_yO_2$ (NCM) cathodes (Piątek et al., 2021). Without proper recycling, the large amounts of metals in the batteries will pose a dual challenge to both environment and resources (Qi et al., 2025; Or et al., 2020; Roy et al., 2022; Yang et al., 2022). Therefore, it is crucial to recover the waste LIBs, especially the cathode materials.

Conventional recycling strategies of spent NCM cathode materials based on the separation techniques mainly include pyrometallurgy and hydrometallurgy (Harper et al., 2019; Leal et al., 2023). In pyrometallurgy, the transition metals in NCM are recovered as alloys through high-temperature smelting reduction and further extracted by electrolysis or chemical separation. Nevertheless, a portion of the lithium volatilizes during the high-temperature treatment, and the remainder enters the complex slag, resulting in the requisition of additional steps for its recovery (Huang et al., 2018; Makuza et al., 2021; Mrozik et al., 2021). While in hydrometallurgy, the targeted elements are completely dissolved in the liquid phase, followed by recovering with a sequential extraction (Jung et al., 2021; Xiao et al., 2020; Yang et al., 2023b; Zhao et al., 2024). Despite differences in these two techniques, both require a multi-stage operation to stepwise separate the targeted elements, resulting in a limited recovery efficiency (Lei et al., 2022).

An alternative strategy for recycling spent NCM cathodes is to directly convert the involved metal components into functional materials, without the separation of transition metals. It is verified that the synergistic effect of transition metals, especially nickel, cobalt, and manganese, could play a positive contribution to the catalytic activity (L. Li et al., 2023; Marquez et al., 2024; Sari et al., 2024; Yu et al., 2018).

* Corresponding authors.
E-mail addresses: zhangzhihao@ucas.ac.cn (Z. Zhang), jingzhang@ucas.ac.cn (J. Zhang).

https://doi.org/10.1016/j.resconrec.2025.108466
Received 15 April 2025; Received in revised form 24 May 2025; Accepted 12 June 2025
Available online 18 June 2025

Recent studies have shown that NCM cathodes can be directly converted into transition metal (hydr)oxides or sulfides, servings as catalysts for the oxygen evolution reaction (OER) and oxygen reduction reaction (ORR), which exhibit great catalytic activity, attributed to improved charge transfer at heterointerfaces and the abundance of active sites provided by high surface areas (M. Chen et al., 2024; Jiao et al., 2022; Chen, 2024; Wei et al., 2018). However, the treatment processes remain complex, due to the multiple leaching and precipitation, which occasionally involve several phase transitions. Moreover, simultaneously achieving the efficient lithium extraction in the direct conversion process continues to be overlooked.

This work presents a novel recycling strategy for the spent NCM cathodes, enabling the selective extraction of lithium and simultaneous conversion of remaining transition metals into the self-supported NCM-OH catalyst. The instantaneous thermal shock, provided by flash joule heating and quenching, enables the formation of the soluble lithium compound and the metastable multimetallic nanoparticles, which can effortlessly reconstruct into the NCM hydroxide film in limited water. Compared with conventional pyrolysis, this method reduces reaction time, improves lithium retention, and enhances structural reactivity. Due to the rapid quenching, 95.89 % of lithium was successfully recovered through a simple water leaching process. The NCM-OH catalyst exhibits excellent OER activity and long-term stability in 1.0 M KOH, with a low overpotential of 257 mV (vs. RHE) at 10 mA/cm^2, attributed to the lower activation energy provided by the multimetallic hydroxide film. The economic-environmental analysis highlights that this approach offers enhanced economic profitability and reduced environmental footprint, as compared with the conventional recycling strategies.

2. Experimental section

2.1. Synthesis of precursor solution

A mixed acid solution was prepared by dissolving H_2SO_4 (0.3923 g) and l-ascorbic acid (LAA) (0.8806 g) in deionized water up to 10 mL. The addition of NCM811 powder (0.4 g) to the solution at 70 °C for a period of 2 h was required to ensure complete dissolution of the NCM811 powder, thus producing the precursor solution SL-45.

2.2. Synthesis of NCM-OH catalyst

The carbon paper was subjected to ultrasonication in acetone, ethanol, and deionized water in a sequential manner for 10 min to remove any impurities or contaminants that may have accumulated on its surface.

SL-45 was added dropwise to the carbon paper at a loading amount of 100 μL/cm^2 and allowed to dry at 80 °C overnight.

The carbon paper, which had been loaded with the precursor solution and dried, was subjected to rapid joule heating (FJH) in a reaction cell filled with Ar gas. The voltage was set to 10 V, the current to 10 A, and the reaction time to 500 ms, causing the temperature to reach approximately 950 °C. The FJH-treated carbon paper was leached using deionized water and then dried at 80 °C for 12 h to obtain NCM-OH catalyst. Lithium ions have been observed to accumulate in the leach solution.

2.3. Electrochemical measurements

All electrochemical measurements were performed on a CHI 660D electrochemical workstation at room temperature (25 °C), using a typical three-electrode cell in 1.0 M KOH (pH = 13.85) electrolyte, with a graphite rod as the counter electrode and a standard Hg/HgO reference electrode (Tianjin Aida Hengsheng Technology Co. Ltd., China).

2.4. DFT calculation

All spin-polarized density functional theory (DFT) calculations were performed by Vienna ab Initio Simulation package (VASP) with Perdew-Burke-Ernzerhof (PBE) exchange correlation functional (Kresse, G., et al., 1996). For van der Waals (vdW) corrections, the DFT-D3 scheme developed by Grimme was employed. Projected augmented wave (PAW) potentials were used to describe the ionic cores, while the valence electrons were represented by a plane-wave basis set with a kinetic energy cutoff of 520 eV (Blöchl, P. E. 1994). The k-point sampling was carried out using the Monkhorst-Pack scheme with a Γ-centered 3 × 3 × 1 grid. The convergence thresholds for energy and force were set to 10^{-7} eV and 0.02 eV/Å.

2.5. Economic and environmental analysis

In order to ascertain the economic and environmental impacts, an EverBatt model produced by Argonne Laboratory was employed to evaluate this experimental method in comparison with pyrometallurgical (Pyro) and hydrometallurgical (Hydro) recovery methods in terms of cost, revenue, energy consumption, and GHGs emission (Dai, 2019). The parameter settings were adjusted and modified based on the default settings in the model.

3. Results and discussion

The experimental process is illustrated in Fig. 1 and consists of four

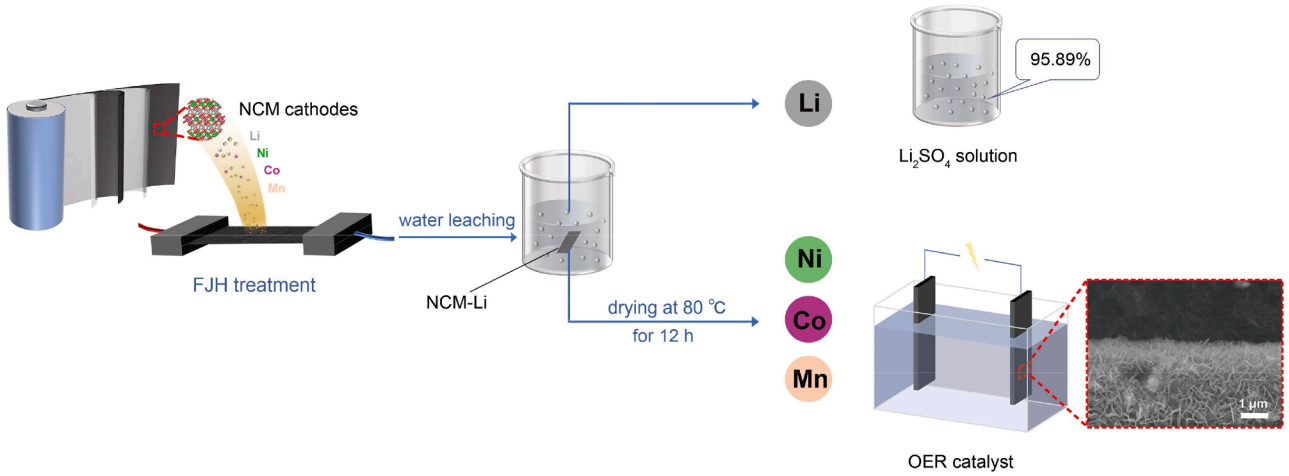

Fig. 1. Schematic diagram of the upcycling NCM cathodes for lithium extraction and NCM-OH catalyst preparation.

steps: acid leaching, reduction roasting, leaching separation and surface reconstruction. First, NCM811 powders were dissolved in the sulfuric acid/L-ascorbic acid (LAA) solution (Fig. S1). The mixed solution was socked on the carbon paper (CP) to obtain the precursor. During the instantaneous thermal shock of flash joule heating (FJH), carbon derived from LAA in the precursor provided a reducing atmosphere, facilitating the reduction of transition metals. As a result, lithium and transition metal compounds were attached onto the CP, forming the raw product (named NCM-Li). Lithium preferentially recovered via leaching separation due to its high solubility in water. The remaining solid containing transition metal elements was then dried at 80 °C. During the process, surface reconstruction occurred on the CP surface, leading to the formation of multimetallic film with a novel structure as the excellent OER catalyst.

3.1. Recovery of lithium

As shown in Fig. 2a, the raw product of NCM-Li is mainly composed of Li_2SO_4, Ni/Co metals and Ni_3S_2 on the carbon paper, as confirmed by XRD analysis. The formation of metal elements and their corresponding sulfides resulted from the reductive environment formed by decomposed carbon species from LAA and the reduced sulfur species generated from SO_4^{2-}. Meanwhile, the absence of characteristic peaks for manganese phases could be attributed to the incorporation of manganese into Ni_3S_2, along with some cobalt, due to their similarity to nickel (Qian et al., 2022; S. Li et al., 2023). The presence of Li_2SO_4 is owing to the relatively stronger thermodynamic stability, which makes it less prone to decomposition or chemical reactions during the instantaneous heating (Yang et al., 2024). Additionally, nanoparticles form undergoes the liquefaction and aggregation of Li_2SO_4 from the SL-45 precursor by the instantaneous thermal shock of FJH (Fig. 2b) (Kotkar et al., 2023; Zhu et al., 2023) . After water leaching, the diffraction peaks of Li_2SO_4 disappear, accompanied by the disappearance of nanoparticles with an average diameter of 50.6 nm on the NCM-OH surface (Fig. 2c). Due to the high solubility of Li_2SO_4, it can be easily extracted through water leaching. Moreover, the characteristic XPS peak of the Li element fades away after washing, again confirming the removal of Li_2SO_4 (Fig. 2d). As a result, lithium can be recovered with an efficiency of 95.89 % through water leaching, based on the ICP-OES analysis of the leachate (Table S1).

3.2. Characteristics of NCM-OH catalyst

After washing to recover Li, the dried product shows a sheet-like film structure covered on the surface of NCM-OH (Fig. 2c, Fig. S3). In addition, multimetallic nanoparticles (including both metals and metal sulfides), with an average diameter of 25.2 nm, are present on the carbon substrate (Fig. S2a-b). The thin film also presents new XRD peaks and can be recognized as $Ni(OH)_2{\cdot}0{\cdot}75H_2O$ (Fig. 2a). As a comparison, the resulting product (named NCM-CP) by rapidly drying shows no thin-film structure, but only dense multimetallic nanoparticles, similar to the underneath bulk phase of NCM-OH (Fig. S2c and S4). It indicates that the metastable multimetallic nanoparticles are partially and slowly dissolved in the limited residual water on the surface. The hydrolysis products undergo a surface reconstruction, resulting in the formation of the hydroxide thin film (Ou et al., 2025). The HRTEM image in Fig. 2e shows the well-defined crystal lattice stripes with a spacing of 0.259 nm, corresponding to the (012) crystal plane of $Ni(OH)_2{\cdot}0{\cdot}75H_2O$. Fig. 2f reveals the elemental composition of the thin film by mapping analysis,

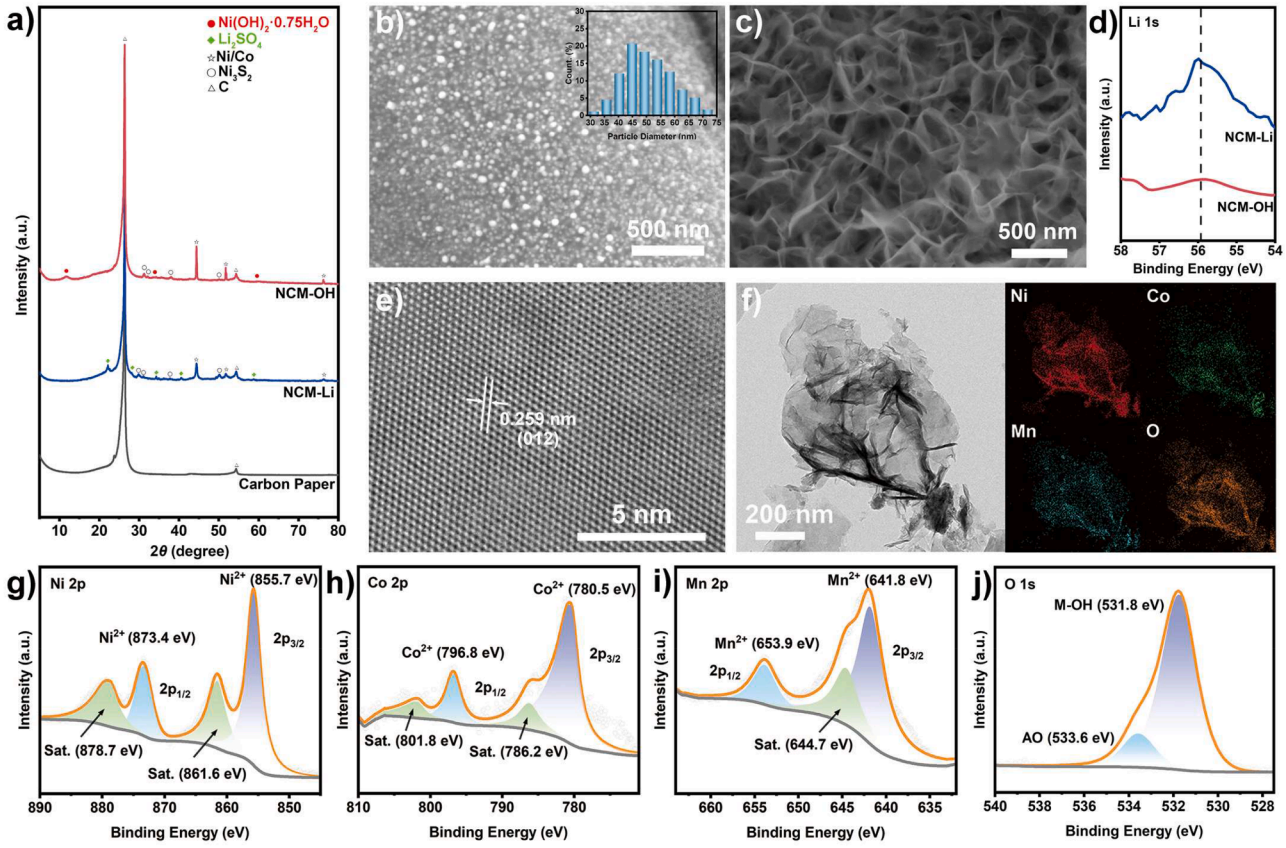

Fig. 2. Characterization of the solid products: (a) XRD of NCM-OH, NCM-Li and carbon paper, (b-c) SEM of NCM-Li (b) (Inset: statistical size distribution of nanoparticles on the surface) and NCM-OH (c), (d) their corresponding XPS of Li 1 s, (e-f) HRTEM (e) and elemental mapping (f) of the multimetallic hydroxide film on the NCM-OH surface, (g-j) XPS spectra of NCM-OH: (g) Ni 2p, (h) Co 2p, (i) Mn 2p, and (j) O 1 s.

where Ni, Co, Mn, and O elements are homogeneous distributed throughout the thin film. It suggests that Co and Mn are doped into the film structure of $Ni(OH)_2{\cdot}0{\cdot}75H_2O$ by replacing the Ni sites.

Fig. 2g-j show the valence states of elements on the film through the XPS analysis. It reveals the XPS spectra of Ni 2p (855.7 eV and 873.4 eV), Co 2p (780.5 eV and 796.8 eV), and Mn 2p (641.7 eV and 653.7 eV) peaks, confirming the presence of Ni^{2+}, Co^{2+}, and Mn^{2+} species. Compared with Ni-OH, a slightly shift of the Ni 2p peak is observed, which can be attributed to the coexistence of Co and Mn in the Ni-based lattice (Fig. S5). Besides, the O 2p spectrum in Fig. 2j exhibits a peak at 531.8 eV associated with M-OH species and another peak at 533.6 eV corresponding to the adsorbed oxygen (Zhu et al., 2020). This suggests that, aside from a small amount of adsorbed oxygen, the oxygen in thin film primarily exists as -OH. On the basis of the above analysis, it can be reasonably deduced that the thin film is composed of the $Ni_{1-x-y}Co_xMn_y(OH)_2{\cdot}0{\cdot}75H_2O$ compound.

3.3. Electrocatalytic performance

The electrocatalytic property of NCM-OH by performing the OER activities in 1.0 M KOH using a standard three-electrode cell. As compared with catalysts synthesized under different acid concentrations, NCM solid-liquid ratios, and FJH temperatures, NCM-OH consistently exhibits the best overpotential and Tafel slope (Fig. S6-S10). From the polarization curves in Fig. 3a, it is clearly observed that the NCM-OH catalyst has an overpotential of 257 mV at 10 mA/cm^2, which is distinctively lower than the control anodes of NCM-CP (295 mV) and IrO_2 (298 mV). The Tafel slopes derived from the corresponding polarization curves show the electrocatalytic kinetics of different catalysts (Fig. 3b). NCM-OH has a much smaller Tafel slope (24.7 mV/dec) than the other two samples of NCM-CP (72.1 mV/dec) and IrO_2 (70.9 mV/dec), indicating the optimal electrochemical kinetics of NCM-OH. The results suggest that NCM-OH with the multimetallic hydroxide film exhibits excellent catalytic activity for OER.

The charge transfer ability and stability of NCM-OH are also important indicators for evaluating the performance of the catalyst. Fig. 3c shows the electrochemical impedance spectroscopy (EIS) for providing the requisite charge transfer information for the catalysts. The charge transfer resistance (R_{ct}) of NCM-OH is 2.26 Ω, while the R_{ct} values of NCM-CP and IrO_2 are 5.14 Ω and 47.84 Ω, respectively. The lower R_{ct} indicates the more efficient charge transfer and the faster interfacial reaction kinetics for NCM-OH. Additionally, compared with the control sample NCM-CP (C_{dl} = 1.00 mF/cm^2), NCM-OH exhibits a higher double-layer capacitance (C_{dl}) of 1.70 mF/cm^2 (Fig. 3d), which directly correlates with a larger electrochemical active surface area (ECSA) of NCM-OH. The results confirm that the thin-film structure of NCM-OH is crucial for enhancing its electrocatalytic activity (Anantharaj et al., 2020).

Furthermore, the chronopotentiometry measurement is shown in Fig. 3e, to assess the stability of NCM-OH. After 120 h of testing at a constant current of 10 mA/cm^2, the overpotential of NCM-OH is increased by only 12 mV, indicating the excellent electrochemical stability. Compared with previously reported transition metal-based catalysts, NCM-OH exhibits a lower overpotential and Tafel slope (Table S2), further confirming its superior OER catalytic performance.

After the stability test, the microstructure of NCM-OH was characterized. As shown in the SEM images (Fig. 4a-b), the surface of NCM-OH exhibites no significant change, retaining its original film-like morphology. Additionally, the XRD pattern of the tested NCM-OH (Fig. 4c) shows peaks consistent with those of the fresh sample, particularly the characteristic peak at 11.3° corresponding to the Ni $(OH)_2{\cdot}0.75H_2O$ phase is well preserved, highlighting its outstanding structural stability under prolonged test. Furthermore, the valence states of the main elements in the tested NCM-OH were analyzed by XPS, and the corresponding Ni 2p, Co 2p, Mn 2p, and O 1 s spectra are shown in Fig. 4d-g, respectively. Based on the XPS peak areas, the transition metals in the tested NCM-OH are primarily in the divalent state, with a small fraction oxidized to the trivalent state. The appearance of peaks at 856.7 and 875.7 eV in Fig. 4d (Konkena et al., 2017), 795.5 and 775.4 eV in Fig. 4e (M. Chen et al., 2024) and 643.8 eV in Fig. 4f (Liu et al., 2021; Wang et al., 2025; Zhang et al., 2021), attributed to Ni^{3+}, Co^{3+} and Mn^{3+} respectively. It suggests partial oxidation of the transition metals

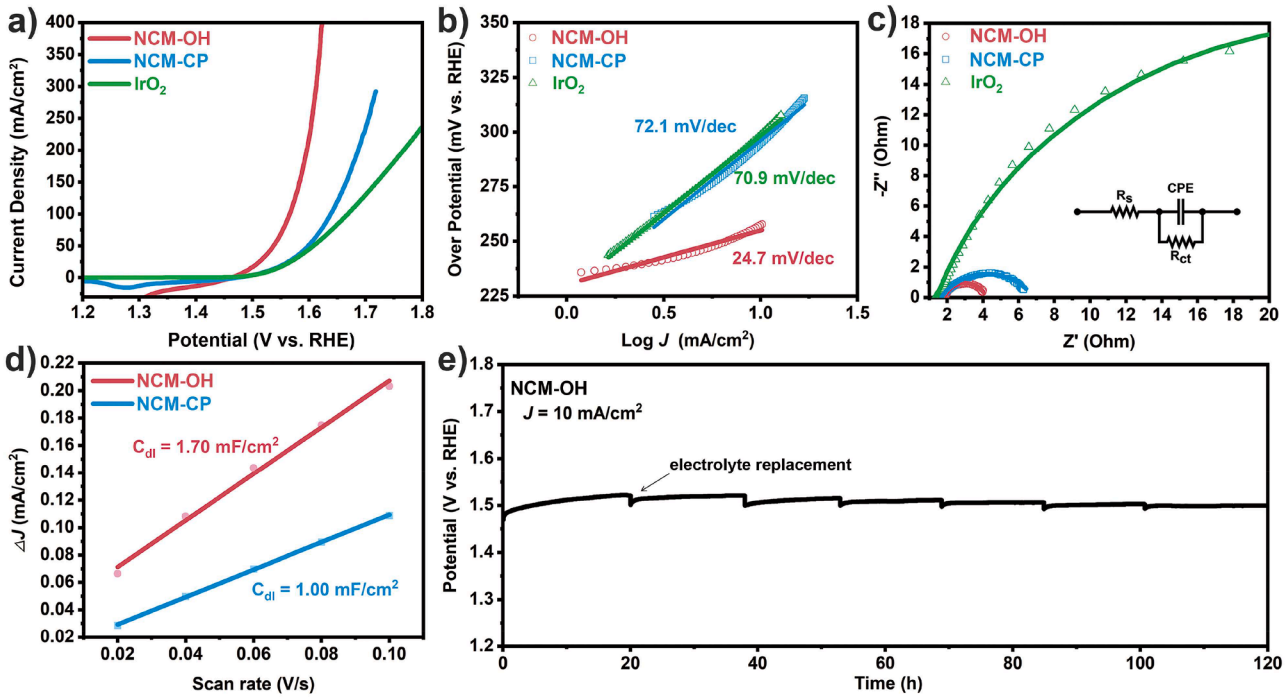

Fig. 3. Electrocatalytic performance of the NCM-OH catalyst test in 1.0 M KOH: (a) OER polarization curves, (b) Tafel slopes derived from the polarization curves, (c) Nyquist plots at 1.555 V (vs. RHE), (d) Double-layer capacitances (C_{dl}), (e) Chrono potentiometry measurement at 10 mA/cm^2. Note that periodic fluctuations in (e) are induced by the electrolyte replacement.

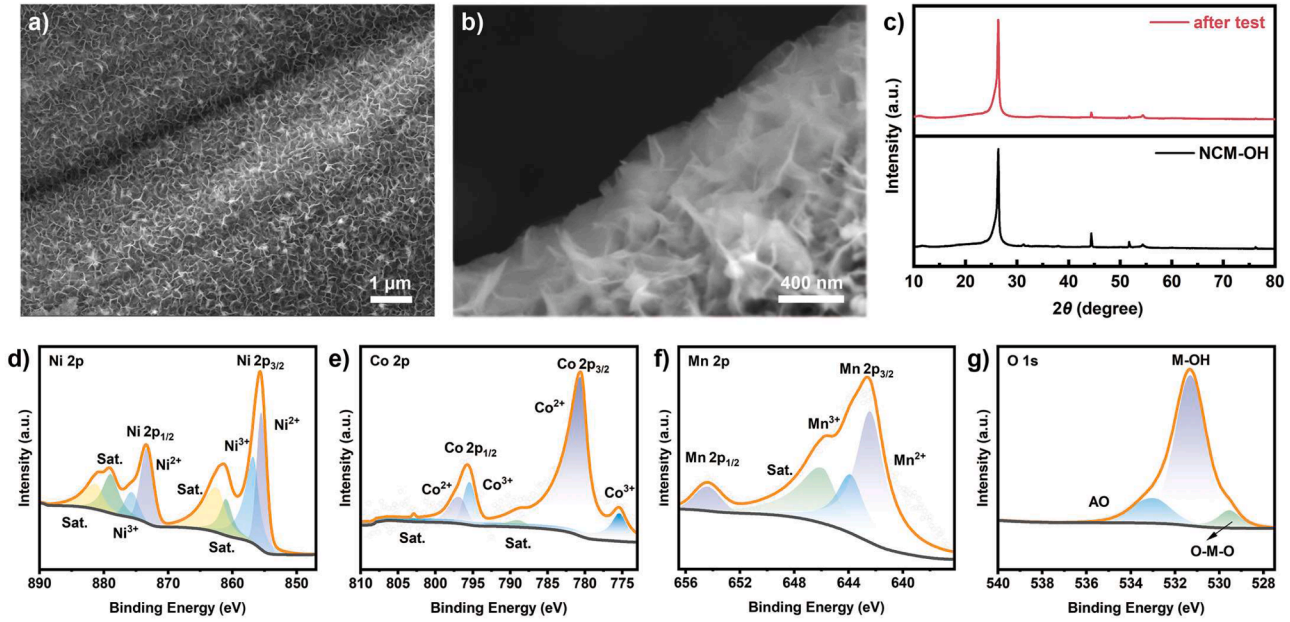

Fig. 4. (a-b) SEM of the tested NCM-OH; (c) XRD of the fresh NCM-OH and the tested NCM-OH; (d-g) XPS spectra of the tested NCM-OH: (d) Ni 2p, (e) Co 2p, (f) Mn 2p, and (g) O 1 s. (stability testing time: 120 h).

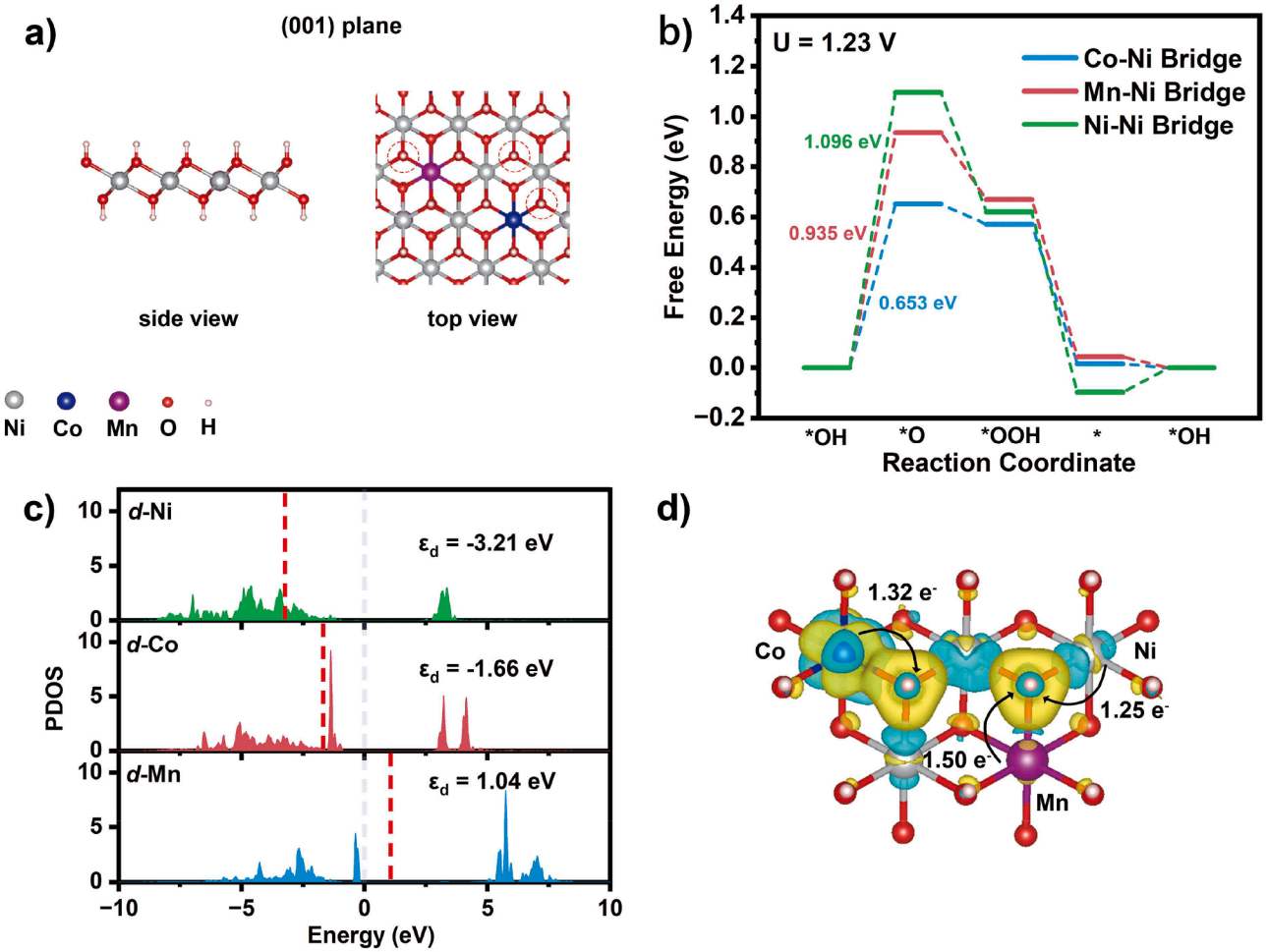

Fig. 5. Theoretical calculation based on DFT for the OER activity of NCM-OH: (a) The computational structure model, where the active sites are marked with circles, (b) Free energy diagram of OER at 1.23 V on the Co-Ni bridge, Mn-Ni bridge, and Ni-Ni bridge, (c) PDOS of *d* band of Ni, Co, and Mn atoms, (d) Charge density difference and Bader charge transfer from Ni, Co and Mn atoms to O atoms. Yellow and blue represent the inflow and outflow of negative charges, respectively.

took place during the stability test, which may be associated with the formation of corresponding oxyhydroxide species. The O-M-O signal at 529.6 eV in the O 1 s spectrum in Fig. 4g further suggest the generation of MOOH intermediates. The valence state evolution observed during the stability test is likely a reversible process associated with the generation of active intermediates, rather than irreversible structural degradation. In conclusion, the NCM-OH catalyst exhibits only minor and reversible surface evolution during the stability test, without any significant structural degradation, demonstrating excellent morphological, structural, and chemical stability under reaction conditions.

3.4. Catalytic mechanism

To reveal the mechanism behind the excellent OER activity of NCM-OH, first-principles DFT calculations were performed by Vienna Ab initio Simulation Package. According to the XRD analysis, a Co- and Mn-doped $Ni(OH)_2$ model was constructed, with the (001) plane selected as the catalytic surface to simulate the film structure (Fig. 5a and Fig. S11-S13). The change of Gibbs free energy (ΔG) for the intermediates, *OH, *O, *OOH, and *, was calculated using the Co-Ni bridge sites, Mn-Ni bridge, and Ni-Ni bridge as the active sites. Since the (001) plane is saturated with -OH, the model with the adsorbed *OH intermediates was used as the initial model to obtain the free energy diagrams (Dionigi et al., 2020). As shown in the free energy diagrams in Fig. 5b and Fig. S14, the *OH to *O step serves as the potential determining step due to its highest reaction energy barrier, which dictates the overall overpotential of the OER reaction. In contrast with the Ni-Ni bridge, which has an overpotential of 1.096 eV, the Co-Ni and Mn-Ni bridges exhibit lower overpotentials of 0.653 eV and 0.935 eV, respectively. This result indicates that the multimetallic hydroxide film reduces the activation energy of the reaction, thereby enhancing the catalytic activity of the anode and lowering the overpotential for the OER reaction.

The *d* band partial densities of states (PDOS) of transition metal atoms are shown in Fig. 5c. The *d* band center of Co atom is at −1.66 eV, which is closer to the Fermi level, compared with that of Ni atom (−3.21 eV). It indicates a reduced occupancy of antibonding states, which will enhance the adsorption capability with -OH. While the *d* band center of Mn atom lies above the Fermi level (1.04 eV), which means that all antibonding orbitals remain unoccupied, and thus preserving bonding interactions and strengthening its bonding ability. Fig. 5d represents the charge density difference and Bader charge for analyzing the bond formation. The charge transfer from Co and Mn to O is 1.32 e and 1.50 e, respectively, while from Ni to O is 1.25 e. The higher charge transfer at the Co and Mn atoms suggests that these active sites exhibit the stronger oxidation properties, which facilitate both the adsorption of -OH and the cleavage of O—H bonds, thereby forming great catalytic activity. This conclusion is further supported by the observed positive shift of the M-OH peak in the O 1 s XPS spectra (Fig. S15). In summary, the doping of Co and Mn enhances the catalytic performance of the multimetallic hydroxide film and thus increases the OER activity of NCM-OH.

4. Economic and environmental analysis

The economic and environmental analysis of recycling NCM cathodes by pyrometallurgy (Pyro), hydrometallurgy (Hydro), and our upcycling strategy (this work) is shown in Fig. 6. Specifically, the costs

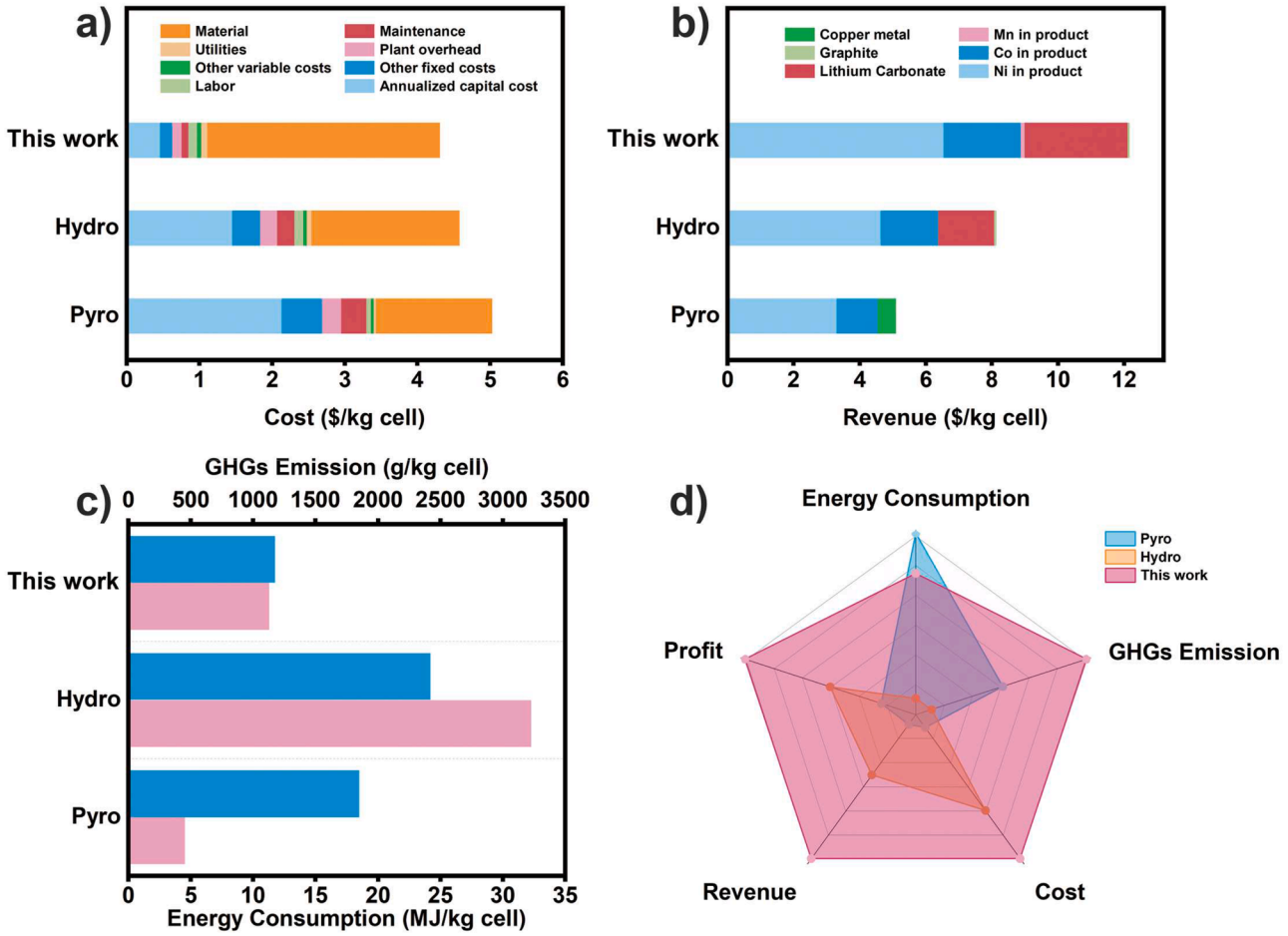

Fig. 6. Economic and environmental analysis of recycling NCM811 cathodes by pyrometallurgy (Pyro), hydrometallurgy (Hydro) and this work: (a) Cost, (b) Revenue, (c) Greenhouse gases (GHGs) emission and energy consumption, (d) Comprehensive comparison of different battery recycling technologies. A larger area enclosed by the curve indicates a higher evaluation.

of recovering 1 kg of NCM 811 are $5.03 for Pyro and $4.58 for Hydro, respectively (Fig. 6a). The recovery cost of this work is relatively low at $4.32, in which a larger proportion of the cost is mainly attributed to the high market price of LAA utilized in the leaching process. In parallel, this work recovers the spent NCM811 cathodes at a higher revenue of $13.18/kg cell, which is 2.58 times that of Pyro ($5.10/kg cell) and 1.62 times that of Hydro ($8.14/kg cell) (Fig. 6b). This is largely attributed to our higher recovery of the valuable metals, particularly lithium, which reaches 185 % of Hydro's revenue. While for Pyro, the model default assumes that lithium either volatilizes or enters the slag, with no recovery considered.

It is also important to consider the environmental impacts in the recycling process. As illustrated in Fig. 6c, the energy consumption of the Pyro and Hydro strategies is 4.53 MJ/kg cell and 32.29 MJ/kg cell, respectively. In comparison, the energy consumption of this work is 11.29 MJ/kg cell, which represents a 65 % reduction relative to the Hydro strategy. Moreover, this work displays a pronounced advantage in GHGs emissions, with a rate of only 1177 g/kg cell. This represents a 64 % reduction (1852 g/kg cell) compared with Pyro and a 49 % reduction (2423 g/kg cell) for Hydro, indicating a markedly reduced carbon footprint of our strategy. The spider diagram illustrates the comprehensive superiority of this work in comparison with Pyro and Hydro recycling strategies (Fig. 6d). It is noteworthy that the EverBatt model does not fully simulate the actual industrial production scenario and should only be used as a reference. However, this work still demonstrates relatively significant advantages over other traditional strategies. Economic and environmental analysis indicates that this work not only has lower recycling costs and higher economic benefits but also reduces secondary pollution, showcasing clear economic advantages and environmental friendliness.

5. Conclusions

In this study, we proposed a flash joule heating-based strategy for upcycling the spent NCM cathodes by concurrently yielding water-soluble lithium compounds and NCM-OH catalyst. It avoids the loss of valuable metals recovery efficiency caused by the complex separation processes. Moreover, the produced NCM-OH catalyst covered with nanostructured thin film of $Ni_{1-x-y}Co_xMn_y(OH)_2{\cdot}0.75H_2O$ presents excellent OER catalytic activity and stability. It reveals that the incorporated Co and Mn in the nano-film significantly promote the oxidation properties of the catalyst. Our upcycling strategy offers significant advantages over the traditional strategies in terms of both economic and environmental aspects. Therefore, this work provides an efficient approach for fully upcycling the spent ternary cathodes via both separation of lithium and manufacturing transition metal-based functional materials.

CRediT authorship contribution statement

Chunli Gou: Writing – original draft, Visualization, Validation, Methodology, Investigation, Formal analysis, Data curation, Conceptualization. **Fang Gao:** Writing – review & editing, Investigation, Data curation. **Mingke Yang:** Writing – review & editing, Investigation, Data curation. **Zhihao Zhang:** Writing – review & editing, Visualization, Methodology, Funding acquisition, Conceptualization. **Chunli Wang:** Writing – review & editing. **Yufang Wang:** Writing – review & editing. **Xinwen Ou:** Software. **Jing Zhang:** Writing – review & editing, Supervision, Resources, Funding acquisition, Conceptualization.

Declaration of competing interest

The authors declare that they have no known competing financial interests or personal relationships that could have appeared to influence the work reported in this paper.

Acknowledgements

This work was supported by the National Natural Science Foundation of China (21876190, 22276192 and 22306183), the Fundamental Research Funds for the Central Universities, and Weiqiao-UCAS Special Projects on Low-Carbon Technology Development (GYY-DTFZ-2022-009).

Supplementary materials

Supplementary material associated with this article can be found, in the online version, at doi:10.1016/j.resconrec.2025.108466.

Data availability

Data will be made available on request.

References

Anantharaj, S., et al., 2020. Amorphous catalysts and electrochemical water splitting: an untold story of harmony. Small 16, 1905779. https://doi.org/10.1002/smll.201905779.
Blöchl, P.E., 1994. Projector augmented-wave method. Phys. Rev. B 50 (24), 17953–17979. https://doi.org/10.1103/PhysRevB.50.17953.
Chen, M., et al., 2019. Recycling end-of-life electric vehicle lithium-ion batteries. Joule 3, 2622–2646. https://doi.org/10.1016/j.joule.2019.09.014.
Chen, M., et al., 2024. Recycling spent $LiNi_{1-x-y}Co_xMn_yO_2$ cathodes to efficient catalysts for the oxygen evolution reaction. Green Chem. 26, 2912–2921. https://doi.org/10.1039/D3GC04503J.
Chen, G., et al., 2024. Recycling the Spent $LiNi_{1-x-y}Mn_xCo_yO_2$ Cathodes for High-Performance Electrocatalysts toward Both the Oxygen Catalytic and Methanol Oxidation Reactions. Small 20 (15), 2306967. https://doi.org/10.1002/smll.202306967.
Dai, Q., et al., 2019. EverBatt: a closed-loop battery recycling cost and environmental impacts model (No. ANL–19/16) 1530874, 153050. https://doi.org/10.2172/1530874.
Dionigi, F., et al., 2020. In-situ structure and catalytic mechanism of NiFe and CoFe layered double hydroxides during oxygen evolution. Nat. Commun. 11, 2522. https://doi.org/10.1038/s41467-020-16237-1.
Harper, G., et al., 2019. Recycling lithium-ion batteries from electric vehicles. Nature 575, 75–86. https://doi.org/10.1038/s41586-019-1682-5.
Huang, B., et al., 2018. Recycling of lithium-ion batteries: recent advances and perspectives. J. Power Sources 399, 274–286. https://doi.org/10.1016/j.jpowsour.2018.07.116.
Jiao, M., et al., 2022. Recycling spent $LiNi_{1-x-y}Mn_xCo_yO_2$ cathodes to bifunctional NiMnCo catalysts for zinc-air batteries. Proc. Nat. Acad. Sci. 119, e2202202119. https://doi.org/10.1073/pnas.2202202119.
Jung, J.C.Y.;, et al., 2021. A review of recycling spent lithium-ion battery cathode materials using hydrometallurgical treatments. J. Energy Storage 35, 102217. https://doi.org/10.1016/j.est.2020.102217.
Khan, F.M., et al., 2023. Design and optimization of lithium-ion battery as an efficient energy storage device for electric vehicles: a comprehensive review. J. Energy Storage 71, 108033. https://doi.org/10.1016/j.est.2023.108033.
Konkena, B., et al., 2017. Metallic $NiPS_3$@NiOOH core–shell heterostructures as highly efficient and stable electrocatalyst for the oxygen evolution reaction. ACS Catal 7, 229–237. https://doi.org/10.1021/acscatal.6b02203.
Kotkar, A., et al., 2023. Microwave assisted recycling of spent Li-ion battery electrode material into efficient oxygen evolution reaction catalyst. Electrochim. Acta 442, 141842. https://doi.org/10.1016/j.electacta.2023.141842.
Leal, V.M., et al., 2023. Recycling of spent lithium-ion batteries as a sustainable solution to obtain raw materials for different applications. J. Energy Chem. 79, 118–134. https://doi.org/10.1016/j.jechem.2022.08.005.
Lei, S., et al., 2022. Solvent extraction for recycling of spent lithium-ion batteries. J. Hazard. Mater. 424, 127654. https://doi.org/10.1016/j.jhazmat.2021.127654.
Li, D., et al., 2022. Temperature prediction of lithium-ion batteries based on electrochemical impedance spectrum: a review. International J. Energy Res. 46, 10372–10388. https://doi.org/10.1002/er.7905.
Li, L., et al., 2023. High valence metals engineering strategies of Fe/Co/Ni-based catalysts for boosted OER electrocatalysis. J. Energy Chem. 76, 195–213. https://doi.org/10.1016/j.jechem.2022.09.022.
Qi, C., et al., 2025. Global and regional patterns of soil metal(loid) mobility and associated risks. Nat. Commun. 16, 2947. https://doi.org/10.1038/s41467-025-58026-8.
Li, S., et al., 2023b. Doped Mn enhanced NiS electrooxidation performance of HMF into FDCA at industrial-level current density. Adv. Funct. Mater. 33, 2214488. https://doi.org/10.1002/adfm.202214488.
Liu, Y., et al., 2021. Porous Mn-doped cobalt phosphide nanosheets as highly active electrocatalysts for oxygen evolution reaction. Chem. Eng. J. 425, 131642. https://doi.org/10.1016/j.cej.2021.131642.

Yang, L., et al., 2023a. Fluorine-Rich supramolecular nano-container crosslinked hydrogel for lithium extraction with super-high capacity and extreme selectivity. Angew. Chem. Int. Ed. 62, e202308702. https://doi.org/10.1002/anie.202308702.
Makuza, B., et al., 2021. Pyrometallurgical options for recycling spent lithium-ion batteries: a comprehensive review. J. Power Sources 491, 229622. https://doi.org/10.1016/j.jpowsour.2021.229622.
Marquez, R.A., et al., 2024. Transition metal incorporation: electrochemical, structure, and chemical composition effects on nickel oxyhydroxide oxygen-evolution electrocatalysts. Energy Environ. Sci. 17, 2028–2045. https://doi.org/10.1039/D3EE03617K.
Mrozik, W., et al., 2021. Environmental impacts, pollution sources and pathways of spent lithium-ion batteries. Energy Environ. Sci. 14, 6099–6121. https://doi.org/10.1039/D1EE00691F.
Or, T., et al., 2020. Recycling of mixed cathode lithium-ion batteries for electric vehicles: current status and future outlook. Carbon Energy 2, 6–43. https://doi.org/10.1002/cey2.29.
Piątek, J., et al., 2021. Sustainable Li-ion batteries: chemistry and recycling. Adv. Energy Mater. 11, 2003456. https://doi.org/10.1002/aenm.202003456.
Qian, G., et al., 2022. Efficient photoreduction of diluted CO_2 to tunable syngas by Ni−Co dual sites through D-band center manipulation. Angew. Chem. Int. Ed. 61, e202210576. https://doi.org/10.1002/anie.202210576.
Roy, J.J., et al., 2022. Green recycling methods to treat lithium-ion batteries E-waste: a circular approach to sustainability. Adv. Mater. 34, 2103346. https://doi.org/10.1002/adma.202103346.
Sari, F.N.I., et al., 2024. Electronic structure engineering in NiFe Sulfide via a third metal doping as efficient bifunctional OER/ORR electrocatalyst for rechargeable zinc-air battery. Adv. Funct. Mater. 34, 2310181. https://doi.org/10.1002/adfm.202310181.
Yang, L., et al., 2022. Closed-loop regeneration of battery-grade $FePO_4$ from lithium extraction slag of spent Li-ion batteries via phosphoric acid mixture selective leaching. Chem. Eng. J. 431, 133232. https://doi.org/10.1016/j.cej.2021.133232.
Wang, Y., et al., 2025. Recycling spent lithium-ion battery cathodes to multimetallic phosphides for high-efficiency oxygen evolution reaction. ACS Sustainable Chem. Eng. 13, 2477–2486. https://doi.org/10.1021/acssuschemeng.4c08960.
Wei, J., et al., 2018. Reuse of Ni-Co-Mn oxides from spent Li-ion batteries to prepare bifunctional air electrodes. Resour. Conserv. Recy. 129, 135–142. https://doi.org/10.1016/j.resconrec.2017.10.021.
Xiao, J., et al., 2020. Challenges to future development of spent lithium ion batteries recovery from environmental and technological perspectives. Environ. Sci. Technol. 54, 9–25. https://doi.org/10.1021/acs.est.9b03725.
Yang, C., et al., 2024. Enhanced selective separation of valuable metals from spent lithium-ion batteries by aluminum synergistic sulfation roasting strategy. Sep. Purif. Technol. 345, 127279. https://doi.org/10.1016/j.seppur.2024.127279.
Yang, L., et al., 2023b. Direct electrochemical leaching method for high-purity lithium recovery from spent lithium batteries. Environ. Sci. Technol. 57, 4591–4597. https://doi.org/10.1021/acs.est.3c00287.
Yu, X.Y., et al., 2018. Mixed metal sulfides for electrochemical energy storage and conversion. Adv. Energy Mater. 8, 1701592. https://doi.org/10.1002/aenm.201701592.
Zhang, Z., et al., 2021. Stacking fault disorder induced by Mn doping in $Ni(OH)_2$ for supercapacitor electrodes. Chem. Eng. J. 412, 128617. https://doi.org/10.1016/j.cej.2021.128617.
Zhao, J., et al., 2024. Coupling electrochemical leaching with solvent extraction for recycling spent lithium-ion batteries. Environ. Sci. Technol. 58, 16803–16814. https://doi.org/10.1021/acs.est.4c06480.
Ou, X., et al., 2025. Quantitative relationship between activity effects and interfacial characteristics of environmental fine particles. Natl. Sci. Rev. NWAF 161. https://doi.org/10.1093/nsr/nwaf161.
Zhu, W., et al., 2020. NiCo/NiCo–OH and NiFe/NiFe–OH core shell nanostructures for water splitting electrocatalysis at large currents. Appl. Catal. B-Environ. 278, 119326. https://doi.org/10.1016/j.apcatb.2020.119326.
Zhu, X.H., et al., 2023. Recycling valuable metals from spent lithium-ion batteries using carbothermal shock method. Angew. Chem. Int. Ed. 62, e202300074. https://doi.org/10.1002/anie.202300074.
Kresse, G., et al., 1996. Efficiency of ab-initio total energy calculations for metals and semiconductors using a plane-wave basis set. Comput. Mater. Sci. 6 (1), 15–50. https://doi.org/10.1016/0927-0256(96)00008-0.